

# Self-Adaptive Differential Evolution for Bio-Inspired Neuromorphic Collision Avoidance

Llewlyn Salt  
 ITEE, University of Queensland  
 St Lucia, Australia  
 Email: llewlyn.salt@uqconnect.edu.au

David Howard  
 Data61, CSIRO  
 Pullenvale, Australia  
 Email: david.howard@data61.csiro.au

**Abstract**—We present the optimisation of a neuromorphic adaptation of a spiking neural network model of the locust *Lobula Giant Movement Detector* (LGMD), which detects looming objects and can be used to facilitate obstacle avoidance in robotic applications. Due to the number of user-defined parameters and the size of the search space, it is difficult to find values that detect looming events and ignore translation. Additionally, evaluation of the objective function is expensive (approximately one minute), the properties of the black box objective function are unknown, and derivatives are not available. Therefore, we investigate the use of Differential Evolution and self-adaptive DE (SADE) to find optimal values. We demonstrate that these optimisation algorithms are suitable candidates to find suitable parameters for an obstacle avoidance system on an unmanned aerial vehicle (UAV).

## I. INTRODUCTION

State of the art artificial systems are less power efficient and robust than their natural counterparts. Indeed, a bee is capable of robust flight, obstacle avoidance, and cognitive capabilities with a brain that only consumes  $10\mu W$  of power. On the other hand, vehicles in the DARPA Desert and Urban challenges consume around  $1kW$  of power [1]. Using nature as inspiration, neuromorphic engineers have attempted to bridge the gap through hardware solutions [1]. Neuromorphic processors, such as the CXQuad described in [2], allow for the hardware implementation of spiking neural networks (SNNs). These chips are low power and could provide an attractive alternative to current hardware used in mobile applications such as robotics.

Another successful neuromorphic solution is the dynamic vision sensor (DVS) [3]. The DVS is analogous to a camera, except instead of integrating light for a period of time and then converting it to an image it detects changes in luminance at microsecond accuracy and transmits these as events at a pixel location [4]. This leads to a reduction in power, bandwidth, and overhead in post processing. A pencil balancing robot was implemented using DVSs and micro-controllers [5]. Due to its high temporal precision the DVS also doesn't suffer from blurring as a standard-frame based camera might when conducting high-speed manoeuvres on an unmanned aerial vehicle (UAV) [6].

High speed agile manoeuvres, such as juggling, pole acrobatics, or flying through thrown hoops use external motion sensors and high powered CPUs to control the UAVs [7], [8],

[9]. A system with sensors and image processing in-situ on the UAV is an essential step for autonomous UAV systems in GPS restricted environments. The authors in [10] investigated the use of a Locust Giant Motion Detector (LGMD) model for collision avoidance in UAVs.

The LGMD model detects whether a stimulus is looming (increasing in size in the field of view) or not [11]. It should be robust to translation, which makes it an ideal candidate for obstacle avoidance. Previous implementations of this model used frame based cameras and simplified neural models for embedded applications [11], [12], [13]. The authors in [10] modified the LGMD neural network (LGMDNN) so that it would work using a DVS and on the aforementioned CXQuad. The model used the Adaptive Exponential Integrate and Fire (AEIF) neuron equations [14].

Coupling the modified LGMDNN with the AEIF neural equations without the adaptation component yields 17 user-defined parameters. Finding ideal parameter values is difficult because the parameter space is large, with the potential for complex interdependencies between parameters. Additionally the objective function is expensive to evaluate (one to five minutes per evaluation on an octa-core CPU). As such, we propose the use of an optimisation algorithm to find parameters that cause the LGMDNN to produce the desired outputs.

Differential Evolution (DE) [15] seems a good choice for our application. DE is a simple and efficient stochastic real-parameter optimisation algorithm. DE has only three user-defined parameters that have well defined effects on the optimisers performance [16], [15], [17]. However, these parameters tend to be problem specific and the parameters that have been found to be good for one problem is not necessarily good for another. Therefore, work has been done to modifying DE so that it is self-adaptive. Self-Adaptive DE (SADE) has been shown to perform as well as or better than DE on benchmarking problems [18], [19].

In this work we discuss how DE was applied to the LGMD model when stimulated by simple and complex DVS recordings on the UAV. This involved developing an objective function that accurately described the desired output of the model. Furthermore, we implemented SADE and showed that it maximised the objective function better than DE, with statistical significance.

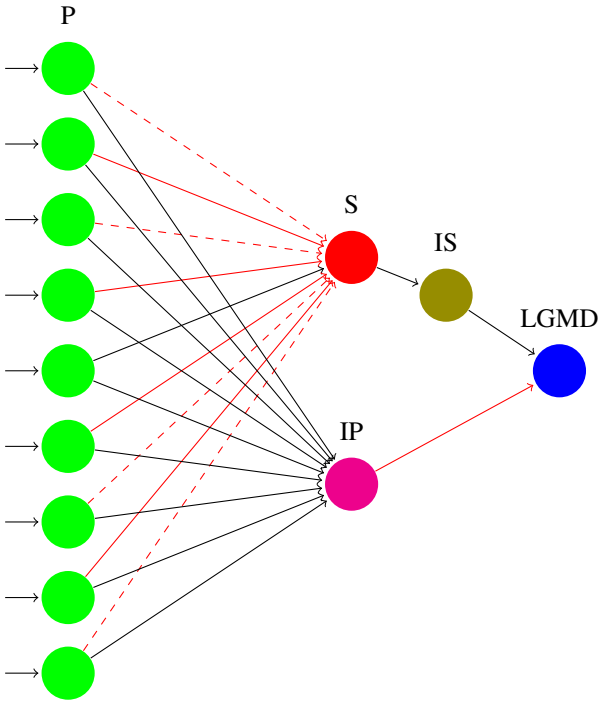


Fig. 1: The neuromorphic LGMD model. Black lines: excitatory connections; red lines: inhibitory connections; dashed lines: slower inhibitions; solid lines: faster inhibitions [10].

## II. LOCUST LGMD MODEL

The LGMDNN was constructed as described in [10]. It consists of the photo-receptors, summing cells, and LGMD output neuron as described in [11]. However, due to constraints on the CXQuad it has intermediate layers to limit the number of synapses coming into a single neuron. Fig. 1 shows the layout of the LGMDNN.

The LGMDNN was implemented in Brian2 neural network simulator due to its documentation, active forums, and purely pythonic implementation. Brian2 will also provide an API for linking with GeNN soon [20], and it also provides a standalone mode which can generate a C++ project from Brian2 Python code [21].

### A. Neuron Equations

The equations used by the optimised model are outlined here. Each neuron in the network was modelled as an Exponential Integrate and Fire (EIF) neuron which is given by:

$$\frac{dV}{dt} = \frac{-g_L(V - E_L) + g_L \Delta_T \exp(\frac{V - V_T}{\Delta_T}) + I_e - I_{iA} - I_{iB}}{C} \quad (1)$$

where  $C$  is the membrane capacitance,  $g_L$  is the leak conductance,  $E_L$  is the leak reversal potential,  $V_T$  is the spike threshold,  $\Delta_T$  is the slope factor,  $V$  is the membrane potential,  $I_e$  is an excitatory current and  $I_{iA}$  and  $I_{iB}$  describe two different types of inhibitory current [14]. When a spike is detected ( $V > V_T$ ) the voltage reset ( $V = V_r$ ) and the post-

synaptic neuron receives a current injections from a pre-neuron firing given by:

$$I_{el+} = q_{el} \quad (2)$$

$$I_{ilA+} = q_{iAl} \quad (3)$$

$$I_{ilB+} = q_{iBl} \quad (4)$$

where  $l$  corresponds to the post-synaptic layer,  $q_{el}$  is a user-defined excitatory current,  $q_{iAl}$  and  $q_{iBl}$  are user-defined fast and slow inhibitory currents. To reduce the range of some of the tunable parameters the inhibitory currents were bound as a ratio of the excitatory current:

$$q_{il(A|B)} = \text{inh}(A|B)_l \cdot q_{el} \quad (5)$$

where the  $(A|B)$  notation indicates either A or B type inhibition.

The decay of the excitatory or inhibitory currents is described by:

$$\frac{dI_a}{dt} = \frac{-I_a}{\tau_a} \quad (6)$$

where  $I_a$  is the current and  $\tau_a$  is the time constant for the decay. The subscript  $a$  refers to either inhibition or excitation.

Fig. 2 shows the output of each layer in the LGMDNN network after using the best optimised parameters to a recording. The recording contained a black circle increasing and decreasing in size and translating left and right on a white background. We can see that the output layer spikes more during non-looming events. This network was not only able to differentiate between objects moving away from and towards the DVS but also translating in front of it.

### B. User-defined Parameters

Assuming that the values can vary from layer to layer but remain homogeneous within that layer would yield 54 user-definable parameters. Fortunately, some of the inherent limitations of the chip reduces this number of parameters:

- $C$ ,  $g_L$ ,  $E_L$ ,  $V_T$ ,  $\Delta_T$  will all be properties of the chip and are therefore kept the same across all layers.
- Each chip containing 1024 neurons can only support two delay constants for each synaptic type so these were also kept the same across all layers.

Each layer could have its own synaptic current strength so this reduced the number of user-defined variables to 17. To reduce the number of parameters further  $C$ ,  $g_L$ ,  $E_L$ ,  $V_T$ ,  $\Delta_T$  were all determined using a greedy parameter space reduction described in [22]. Manually tuning this many user-defined parameters is difficult and time consuming. Many of the variables are not independent, changing values in one layer can change the behaviour in the subsequent layers. Little research on optimising spiking neural networks was found and it seemed like this would be of benefit in this space.

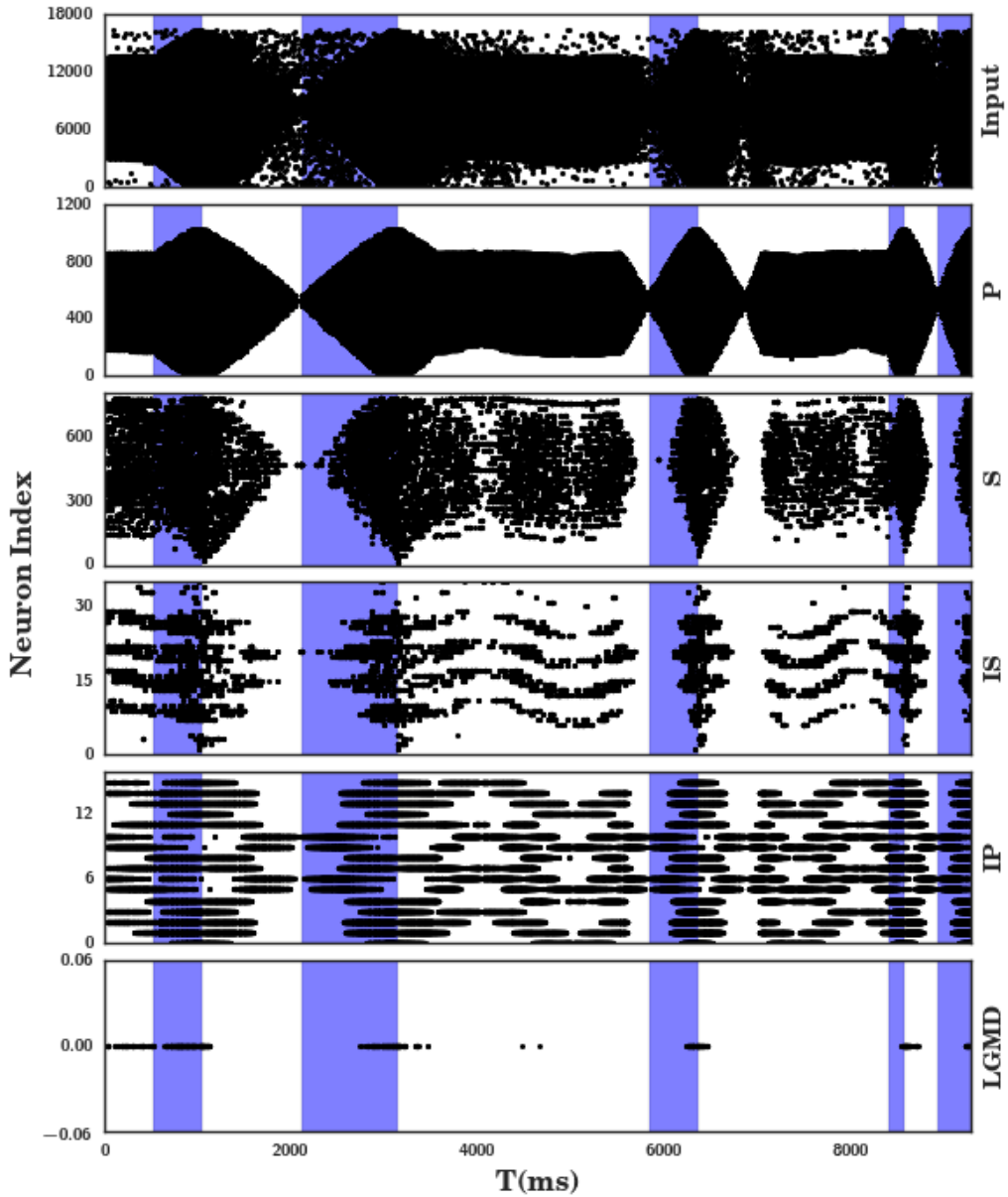


Fig. 2: The input used for the optimisation of the LGMDNN. Each image shows a raster plot of the output of each layer. The purple sections indicate looming and the white sections are non-loom stimuli.

### III. OPTIMISATION

DE was an ideal candidate, for this problem, due to its capability at optimising real-parameters and its simplicity [16], [15]. The inherent properties in the DE algorithm make it an ideal candidate [15]:

- As it is a stochastic direct search method it can solve non-differentiable, non-linear, and multi-modal objective functions.
- It can be parallelised because each vector in the population can be randomly altered independently.
- Using only three user-defined parameters with well known effects on the performance on the optimiser in-

creases its usability.

- It consistently converges to a global minimum or maximum in consecutive independent trials.

These properties are ideal when optimising the LGMDNN model as the surface of the objective function is largely unknown, each simulation takes anywhere from 30 seconds to 4 minutes, and the user-parameters of the model are not as intuitive as DE's.

#### A. Differential Evolution

DE performs a parallel direct search over a population of size,  $NP$ ,  $D$ -dimensional vectors for each generation  $G$ :

$$x_{i,G} = 1, 2, \dots, NP \quad (7)$$

The initial population is generated from random samples drawn from a uniform probability distribution of the parameter space. The fitness of each vector in the population is then calculated by the objective function.

Over each generation each vector is mutated by:

$$v_{i,G+1} = x_{r_1,G} + F \cdot (x_{r_2,G} - x_{r_3,G}) \quad (8)$$

with random indexes  $r_1 \neq r_2 \neq r_3 \neq i \in [1, NP]$ , and  $F \in [0, 2]$ .

Once the mutated vector is generated it undergoes crossover to maintain diversity. The new vector  $u_{i,G+1} = (u_{1i,G+1}, \dots, u_{Di,G+1})$  is found by:

$$u_{ji,G+1} = \begin{cases} v_{ji,G+1}, & \text{if } \text{rand}(j) \leq CR \text{ or } j = R \\ x_{ji,G}, & \text{otherwise} \end{cases} \quad (9)$$

where  $j \in (1, \dots, D)$ ,  $CR \in [0, 1]$  is the crossover constant,  $\text{rand}(j) \in [0, 1]$  is a uniform random number generator, and  $R \in (1, \dots, D)$  is a randomly chosen index to ensure at least one parameter changes.

The value of index  $i$  is then calculated as:

$$x_{i,G+1} = \begin{cases} u_{i,G+1}, & \text{if } f(u_{ji,G+1}) > f(x_{i,G}) \\ x_{i,G}, & \text{otherwise} \end{cases} \quad (10)$$

Eq. (8) is not the only mutation scheme of the DE algorithm. To differentiate between different DE algorithms they follow the notation:  $DE/x/y/z$ .  $x$  denotes the vector to be mutated (in this case a random vector),  $y$  denotes the number of vectors used, and  $z$  denotes the crossover method (bin for binomial experiments in Eq. (8)). Using this nomenclature gives  $DE/\text{rand}/1/\text{bin}$ . Storn and Price [15] showed that  $DE/\text{rand}/1/\text{bin}$  outperformed several other stochastic minimisation techniques in benchmarking tests.

Whilst the user-defined parameters of DE are intuitive, poor selection can lead to poor performance and the selection is problem dependent [18]. Additionally, each mutation scheme is better suited to different problems. Qin et al. presents a self-adaptive version of DE that selects the  $F$  and  $CR$  variables and mutation schemes based on values that have been successful during a learning phase.

## B. Self-Adaptive DE

The authors of [19], [18] suggest self adaptive DE (SADE) which selects the  $F$  and  $CR$  user-defined variables dynamically during the optimisation process.

The authors in [18] present a simple algorithm that randomly changes  $F$  and  $CR$  with a probability of  $\tau_1$  or  $\tau_2$  respectively. Using the same notation as the previous subsection the new control parameters can be found by:

$$F_{i,G+1} = \begin{cases} 0.1 + 0.9r_1, & \text{if } r_2 < \tau_1 \\ F_{i,G}, & \text{otherwise} \end{cases} \quad (11)$$

$$CR_{i,G+1} = \begin{cases} r_3, & \text{if } r_4 < \tau_2 \\ CR_{i,G}, & \text{otherwise} \end{cases} \quad (12)$$

Where  $r_{1,2,3,4}$  are random numbers generated by a uniform distribution,  $U([0, 1])$ . In their experiments the authors set  $\tau_1 = \tau_2 = 0.1$  so as not to exchange the two old control parameters for two new ones [18]. The authors bound  $F$  to the interval  $[0.1, 1]$  based on their own results and those found by other authors. The lower bound was primarily to stop  $F = 0$  which would result in no mutations. The authors used Eq. (8) as their mutation equation.

Using this somewhat simple alteration of the DE algorithm the authors found that self adaptation performed better, or as well as, standard DE and EA from the literature. They found that it performed better than another adaptive DE called fuzzy adaptive DE.

The authors in [19] expanded on SADE by extending the adaptation to select the mutation strategies over a learning period  $LP$ . The authors selected four mutation strategies (all variables maintain the same meaning as those in Eq. (8) unless otherwise stated):

**DE/rand/1/bin:** demonstrates slow convergence and has strong exploration capabilities. It is described by Eq. (8).

**DE/rand-to-best/2/bin:** usually has fast convergence and operate on uni-modal problems but tend towards local maxima or minima. It can be calculated by:

$$u_{ji,G+1} = \begin{cases} x_{ji,G} + F \cdot (a + b + c), & \text{if } \text{rand}(j) \leq CR \text{ or } j = R \\ x_{ji,G}, & \text{otherwise} \end{cases} \quad (13)$$

where  $a = (x_{best,G} - x_{ji,G})$ ,  $b = (x_{r_1,G} - x_{r_2,G})$ , and  $c = (x_{r_3,G} - x_{r_4,G})$ .  $x_{best}$  is the agent in the population with the current best score.

**DE/rand/2/bin:** has good exploration capabilities due to its Gaussian like perturbation and can be calculated by:

$$u_{ji,G+1} = \begin{cases} x_{r_1,G} + F \cdot (a + b), & \text{if } \text{rand}(j) \leq CR \text{ or } j = R \\ x_{ji,G}, & \text{otherwise} \end{cases} \quad (14)$$

where  $a = (x_{r_2,G} - x_{r_3,G})$  and  $b = (x_{r_4,G} - x_{r_5,G})$ .

**DE/current-to-rand/1:** is rotationally invariant and is calculated by:

$$U_{i,G+1} = X_{i,G} + K \cdot (X_{r_1,G} - X_{i,G}) + F \cdot (X_{r_2,G} - X_{r_3,G}) \quad (15)$$

where  $K \sim U([0, 1])$ , and the capitalised letters indicate vectors as there is no binomial cross-over rate used in this case [23]. The authors stipulate that the strategy pool should be restrictive so as not to introduce unfavourable effects from inappropriate or problem specific strategies and be diverse so as to solve a range of problems [19].

The strategy for a given candidate is selected based on a probability distribution determined by the success rate of a given strategy over the  $LP$ . A strategy is considered successful when it improves the candidate's value. The probabilities of the candidates are initialised as  $\frac{1}{K}$  where  $K$  is the number of strategies being used. After the  $LP$  the probabilities can be calculated by:

$$p_{k,G} = \frac{S_{k,G}}{\sum_{k=1}^K S_{k,G}} \quad (16)$$

where:

$$S_{k,G} = \frac{\sum_{g=G-LP}^{G-1} ns_{k,G}}{\sum_{g=G-LP}^{G-1} ns_{k,G} + \sum_{g=G-LP}^{G-1} nf_{k,G}} + \epsilon \quad (17)$$

where  $k = 1, \dots, K$ ,  $G > LP$ ,  $\epsilon = 0.01$ , and  $ns_{k,G}$  and  $nf_{k,G}$  are the number of successes and failures for a given strategy,  $k$ , in a given generation,  $G$ , respectively. After the  $LP$  is over the strategy probabilities are updated and thus the solution will adapt to the strategy best suited to finding a given problems global optimum.

For the user-defined variables  $CR$  and  $F$  the authors state that  $CR$  is more sensitive to characteristics of the problem and that  $F$  can be seen to relate to convergence speed [19]. Due to  $CR$  being problem dependent, the authors also adapt this based on memory. Before  $G > LP$   $CR$  is calculated by randomly selecting a number from a normal distribution,  $N(0.5, 0.1)$ , with a mean of 0.5 and a standard deviation of 0.3. Afterwards it is calculated by a random number from  $N(CR_{mk}, 0.1)$  where  $CR_{mk}$  is the median value of the successful  $CR$  values for each strategy  $K$ .  $F$  is simply selected from a normal distribution  $N(0.5, 0.3)$ , which will cause it fall on the interval  $[-0.4, 1.4]$  with a probability of 0.997 [19].

The authors tested their algorithm against standard DE algorithms and three other adaptive DE algorithms and found that it generally scored higher, was more stable, and were more likely to converge. Moreover they varied the learning period from 20 to 60 generations and found that changing it between these values did not reduce or increase the effectiveness of the algorithm. This means that there is not an additional user-defined variable to select in  $LP$ . In our implementation of SADE we selected  $F$  to also be selected in the same way as  $CR$  so that the successful  $F$  values could also be learnt.

### C. Objective Function

The objective function is simply a black box function where the goal is to minimise the misclassification rate which is given by [24]:

$$f(\lambda) = \frac{1}{k} \sum_{i=1}^k \mathcal{L}(A_\lambda, D_{train}^i, D_{valid}^i) \quad (18)$$

where  $A_\lambda$  is a machine learning algorithm  $A$  using the hyper-parameters  $\lambda$ ,  $k$  is the number of folds in the cross fold validation,  $\mathcal{L}$  is the misclassification function, and  $D_{train}$  and  $D_{valid}$  are the training and validation datasets respectively.

This is straight forward for models that have a well defined loss function, e.g., that has labels for each data point. However, with a spiking neural network the intended spiking behaviour may not be so obvious. It is possible to monitor the membrane potential of a neuron, the number of spikes, or the spiking rate.

Accuracy or error rates work well when a reasonably continuous function can be generated. However, in this case, increasing simulation time increased the time taken exponentially. Therefore, the network was optimised over four discrete looming and non-looming events. This meant that if accuracy

was the metric chosen to evaluate the function, all candidate solutions would fall into five discrete bins (0, 25, 50, 75 and 100 percent). Particularly for DE and SADE, where the candidates in the population are only replaced in a greedy fashion this could result in the children never being selected to replace the parent. In addition, the performance benefited from having some measure of LGMD neuron output signal as a sanity check to stop the neuron behaviour from becoming unrealistic.

We will not provide an in depth discussion on the objective function, instead we encourage the interested reader to review [22]. The objective function was given by the fitness function incorporating the accuracy given the user-defined parameter vector  $\lambda$ ,  $F_{Acc}(\lambda)$ :

$$F_{Acc}(\lambda) = \begin{cases} 2 \times F(\lambda), & \text{if } F(\lambda) > 0 \text{ and } Acc = 1 \\ Acc \times F(\lambda), & \text{if } F(\lambda) > 0 \\ 0, & \text{if } Acc = 1 \text{ and } F(\lambda) < 0 \\ F(\lambda), & \text{Otherwise} \end{cases} \quad (19)$$

where  $Acc$  is the accuracy of the LGMDNN output and  $F(\lambda)$  is the fitness function.

To calculate the accuracy we needed to know whether or not the LGMDNN had detected looming or not. The LGMD network was said to have detected a looming stimulus if the output neuron's spike rate exceeded a threshold  $SL$ . This can be formalised by:

$$Looming = \begin{cases} \text{True}, & \text{if } SR > SL \\ \text{False}, & \text{Otherwise} \end{cases} \quad (20)$$

where  $SR$  can be calculated by:

$$SR = \sum_{i=t}^{t+\Delta T} S_i \quad (21)$$

where  $\Delta T$  is the time over which the rate is calculated and  $S_i$  is whether or not there is a spike at time  $i$  which is defined as happening if, at time  $i$ , the membrane potential exceeds a threshold.

The looming outputs are then categorised into true positives ( $TP$ ), false positives ( $FP$ ), true negatives ( $TN$ ), and false negatives ( $FN$ ). The accuracy of the output can then be calculated as:

$$Acc = \frac{TP + TN}{TP + TN + FP + FN} \quad (22)$$

$F(\lambda)$  can be calculated by:

$$F(\lambda) = \frac{Score(\lambda) + SSEOS(\lambda)}{2} \quad (23)$$

Where  $Score$  is a scoring function based on the timing of spiking outputs and  $SSEOS$  is the sum squared error of the output signal.

The score is calculated by difference of the penalty and reward function's sums over the simulation:

$$Score(\lambda) = \sum_{i=1}^N R_i - \sum_{i=1}^N P_i \quad (24)$$

The reward can at a given time be calculated by:

$$R(t) = \begin{cases} k \exp(\frac{t}{\Delta t}) + 1, & \text{if looming and spike} \\ 0, & \text{otherwise} \end{cases} \quad (25)$$

The punishment can be calculated by:

$$P(t) = \begin{cases} (l - c) \frac{t}{\Delta t} + c, & \text{if not looming and spike and } t \leq \frac{\Delta t}{2} \\ (l - c) \frac{1 - (t - \frac{\Delta t}{2})}{\Delta t} + c, & \text{if not looming and spike and } t > \frac{\Delta t}{2} \\ 0, & \text{otherwise} \end{cases} \quad (26)$$

In these equations  $t$  and  $\Delta t$  remain consistent with the other objective functions and  $k$ ,  $l$ , and  $c$  are all adjustable constants to change the level of punishment or reward.

To calculate  $SSEOS(\lambda)$  signal was first processed so that every spike had the same value. This was done so that the ideal voltage and the actual voltage would match in looming regions, as the voltage can vary for a given spike. Ultimately, the only concern is that it has crossed the spiking threshold. In the non-looming region the ideal signal was taken to be the resting potential, which was negative for the AEIF model equation. The signal error was calculated at every time step and given by:

$$SSEOS(\lambda) = - \sum_{i=1}^N (V_{actual}^i - V_{ideal}^i)^2 \quad (27)$$

$V_{actual}$  could be obtained directly from the Brian2 state monitor object of the LGMD output neuron,  $N$  in this case is the length of the simulation, and  $i$  indicated each recorded data point at each time step of the simulation.  $V_{ideal}$  was given by:

$$V_{ideal} = \begin{cases} V_{spk}, & \text{if looming} \\ V_r, & \text{otherwise} \end{cases} \quad (28)$$

where  $V_{spk}$  is the normalised value given to each spike and  $V_r$  is the resting potential.

The optimising algorithms were then used to maximise  $F_{acc}(\lambda)$ :

$$F_{acc} = \arg \max_{\lambda} (F_{acc}(\lambda)) \quad (29)$$

#### IV. RESULTS AND DISCUSSION

##### A. Comparison of DE and SADE

DE and SADE were evaluated thirty times on the same input stimulus, so that they could be statistically compared.

The input stimulus included a black circle on a white background performing a short translation to the right, followed by a half loom, a full recession, and then a full loom (The first two non-loom to loom transitions of the composite stimulus). The stimulus was selected because it consisted of a 50:50 looming to not looming ratio. The values of the user defined parameters were selected as:

- DE:  $NP = \frac{10dim}{3}$ ,  $F = 0.6607$ ,  $CR = 0.9426$  from [17]
- SADE:  $LP = 3$ ,  $NP = \frac{10dim}{3}$  where  $dim$  is the number of hyper parameters.

The tests were run using the neuromorphic LGMDNN model. DE and SADE were defined as having converged if they had not improved for three generations. The population size is two more than what is recommended by [17] for the DE algorithm. This size was chosen as it is relatively small and time was an issue. The short convergence meant that the SADE algorithm needed to have a short LP. The processor time was not included as a metric for this as the tests were run on three different computers so the results would not have been reliable.

Table I shows that the SADE algorithm achieved the best fitness, accuracy, precision, and specificity. The DE algorithm achieved the best sensitivity.

TABLE I: Optimisation algorithm metrics.

Method	Fit.	Eval. #	Acc.	Sens.	Prec.	Spec.
DE	-675.44	238.80	0.62	<b>0.65</b>	0.76	0.59
SADE	<b>-84.91</b>	253.20	<b>0.66</b>	0.45	<b>0.88</b>	<b>0.87</b>

Table II shows the statistical significance of the results from Table I. The method in the comparison column is compared to each method in the subsequent column. A + indicates statistically significant values and a . indicates no statistical significance. Statistical significance was defined as  $p \leq 0.05$ . The Mann-Whitney U test was used to determine statistical significance because unlike the t-test it doesn't assume a normal distribution. The Mann-Whitney U test from the scipy library was used to for this analysis.

TABLE II: Comparison of the statistical significance of the results.

SADE	Fit.	Eval. #	Acc.	Sens.	Prec.	Spec.
DE	+	.	+	+	+	+

All of the results were found to be statistically significant besides the small difference in the number of evaluations performed before convergence.

A possible reason that DE underperformed is that the  $F$  values provided in [17] are not appropriate for this problem. The population size may have also been too small. Before the SADE algorithm was implemented, doubling the recommended population size made DE find better results than when it had a smaller population. When the population size is too small, whole regions of the parameter space can be missed resulting in poor performance.

Not a lot of time was spent finding appropriate  $F$ ,  $CR$ , and  $NP$  values to make it perform well. SADE removes the need to find control parameters and has been shown to perform as well or better than DE even when the control parameters are well selected [19]. The generalisability that comes with finding the right control parameters on-the-fly is also appealing.

The addition of the various mutation functions to SADE also seem to help it find better results. This is probably due to the desirable properties of each mutation function cancelling out the others undesirable properties.

It is important to note that in these tests both DE and SADE were able to find 100% accurate values and that these results are the means over 30 tests so that statistical significance could be measured.

### B. Analysis of learned SADE variables

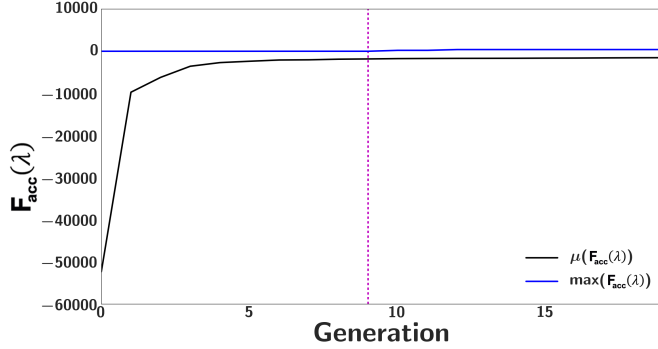


Fig. 3: The average  $F_{acc}(\lambda)$  of a SADE population over 19 generations

The SADE algorithm performed the best out of all of the algorithms. Fig. 3 shows the average  $F_{acc}(\lambda)$  of the population over 19 generations. The average  $F_{acc}(\lambda)$  converged by five iterations. The max  $F_{acc}(\lambda)$  starts off at 0. This indicates that a 100% accuracy candidate was found in the initialisation period. The max  $F_{acc}(\lambda)$  then rises to 400 which is not visible as the range of the average score is -50000 to -1500.

The  $F$  average results in Fig. 4 are interesting. They start off at 1 as they are selected from  $U([0, 2])$  and then drop down to 0.5 as they are selected from  $U([0, 1])$  after the first generation. Once the learning period has finished all of the  $F$  values have converged to less than 0.1. This indicates that the  $F$  values that are having the most success are small and therefore taking advantage of exploration rather than exploitation. It was unexpected that the algorithm would find a min/max within so few generations. This could be why the authors select  $F$  from  $N(0.5, 0.3)$  forcing  $F$  to range from -0.4 to 1.4. With  $F$  this small the algorithm would effectively be performing gradient descent. However, this could be because the function on the restricted space doesn't have many local maxima. Indeed, these results do come from the best performing IL model found.

Fig. 5 shows how the CR for each function changes over time. For the first nine generations the CR values are selected from  $U([0, 1])$  and so the mean stays at 0.5. However, as with the  $F$  mean values once the learning period is over all of the CR values go down to less than 0.1. This means that less than 10% of the mutations will generally take place. From a set of 11 hyper-parameters this means that probabilistically one value will change in addition to the random index that is chosen.  $CR$  is generally associated with convergence.

The probability of each function being chosen is shown in Fig. 6. The probabilities are fixed at 0.25 for the first 9 generations and then they vary based on their success. It

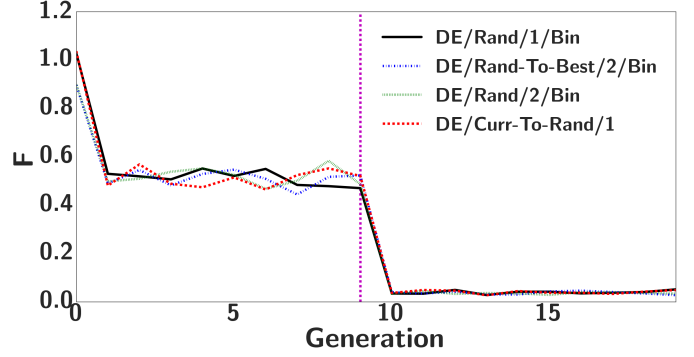


Fig. 4: The average  $F$  for each mutation function of a SADE population over 19 generations

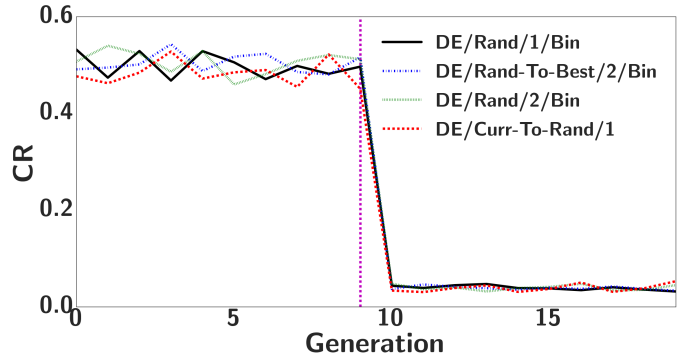


Fig. 5: The average  $CR$  for each mutation function of a SADE population over 19 generations

is interesting to see that in spite of the  $F$  and  $CR$  values suggesting that the algorithm is converging on a solution the DE/Rand-to-Best/2/Bin algorithm is the least successful. The DE/Curr-to-Rand/1 algorithm performs well until about 16 generations where it tapers off. The DE/Rand/2/bin algorithm dips initially but then increases as DE/Curr-to-Rand/1 starts to drop off. The DE/Rand/1/bin remains high during the entire algorithm only to be overtaken by The DE/Rand/2/bin in the last generation.

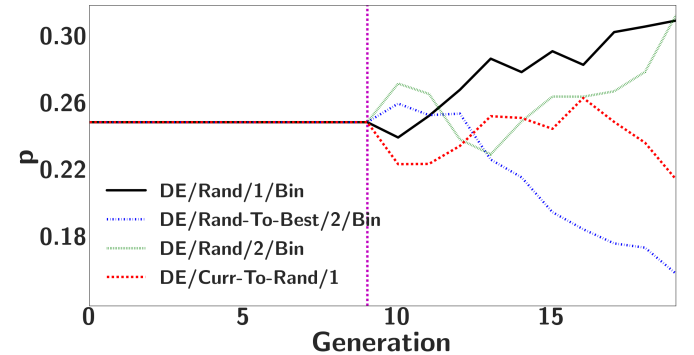


Fig. 6: The average  $p$  of each mutation function of a SADE population over 19 generations

## V. CONCLUSIONS

We implemented a neuromorphic model of the locust LGMD network using recordings from a UAV mounted with a DVS sensor as inputs. The neuromorphic LGMDNN was capable of differentiating between looming and non-looming stimuli. It was capable of detecting the black and white simple stimuli correctly regardless of speed and shape. Real-world stimuli required re-optimisation due to the noise and irregularity of shapes.

We showed that both DE and SADE are capable finding variable values that give the desired performance in the LGMDNN model. It can be seen that SADE statistically significantly outperformed DE on all metrics besides sensitivity and the number of evaluations. Although, the only metrics that formed part of the objective function were fitness and accuracy. Once a suitable objective function was found that accurately described the desired output of the LGMDNN, DE and SADE outperformed hand-crafted attempts. Both algorithms were able to achieve 100% accuracy on complex black and white simple stimuli of varying shapes and speeds. SADE performed well in this task and we have shown that it is suitable for the optimisation of a multi-layered LGMD spiking neural network. This could save time when developing biologically plausible SNNs in related applications.

In the future we would like to apply the optimisation algorithms directly to tuning the neuromorphic processors using the neuromorphic model, with the end goal being a closed loop control system on a UAV. Showing that optimisation is effective for selecting parameters on neuromorphic hardware will increase their usability.

## VI. ACKNOWLEDGMENTS

The neuromorphic model was constructed as part of a master's thesis undertaken at INI. All of the data collection was taken using their sensors and on the institution's UAV. Giacomo Indiveri and Yulia Sandamirskaya assisted on the project and co-authored the LGMDNN model paper with Llewlyn Salt [10].

## REFERENCES

- [1] S. C. Liu and T. Delbrück, "Neuromorphic sensory systems," *Current Opinion in Neurobiology*, vol. 20, no. 3, pp. 288–295, 2010.
- [2] G. Indiveri, F. Corradi, and N. Qiao, "Neuromorphic architectures for spiking deep neural networks," in *2015 IEEE International Electron Devices Meeting (IEDM)*. IEEE, 2015, pp. 4–2.
- [3] T. Serrano-Gotarredona and B. Linares-Barranco, "A  $128 \times 128$  1.5% contrast sensitivity 0.9% FPN 3  $\mu$ s latency 4 mW asynchronous frame-free dynamic vision sensor using transimpedance preamplifiers," *IEEE Journal of Solid-State Circuits*, vol. 48, no. 3, pp. 827–838, 2013.
- [4] T. Delbrück, "Frame-free dynamic digital vision," in *Proceedings of Int'l. Symp. on Secure-Life Electronics, Advanced Electronics for Quality Life and Society*, 2008, pp. 21–26.
- [5] J. Conradt, M. Cook, R. Berner, P. Lichtsteiner, R. J. Douglas, and T. Delbrück, "A pencil balancing robot using a pair of AER dynamic vision sensors," *Proceedings - IEEE International Symposium on Circuits and Systems*, pp. 781–784, 2009.
- [6] E. Mueggler, B. Huber, and D. Scaramuzza, "Event-based, 6-dof pose tracking for high-speed maneuvers," in *2014 IEEE/RSJ International Conference on Intelligent Robots and Systems*. IEEE, 2014, pp. 2761–2768.
- [7] M. Müller, S. Lupashin, and R. D'Andrea, "Quadrocopter ball juggling," in *2011 IEEE/RSJ International Conference on Intelligent Robots and Systems*. IEEE, 2011, pp. 5113–5120.
- [8] D. Brescianini, M. Hehn, and R. D'Andrea, "Quadrocopter pole acrobatics," in *2013 IEEE/RSJ International Conference on Intelligent Robots and Systems*. IEEE, 2013, pp. 3472–3479.
- [9] D. Mellinger and V. Kumar, "Minimum snap trajectory generation and control for quadrotors," in *Robotics and Automation (ICRA), 2011 IEEE International Conference on*. IEEE, 2011, pp. 2520–2525.
- [10] L. Salt, G. Indiveri, and S. Yulia, "Obstacle avoidance with LGMD neuron : towards a neuromorphic UAV implementation ." in *International Symposium on Circuits and Systems*, 2017.
- [11] R. D. Santer, R. Stafford, and F. C. Rind, "Retinally-generated saccadic suppression of a locust looming-detector neuron: investigations using a robot locust," *Journal of The Royal Society Interface*, vol. 1, no. 1, pp. 61–77, 2004.
- [12] S. Yue, R. D. Santer, Y. Yamawaki, and F. C. Rind, "Reactive direction control for a mobile robot: a locust-like control of escape direction emerges when a bilateral pair of model locust visual neurons are integrated," *Autonomous Robots*, vol. 28, no. 2, pp. 151–167, 2010.
- [13] R. Stafford, R. D. Santer, and F. C. Rind, "A bio-inspired visual collision detection mechanism for cars: combining insect inspired neurons to create a robust system," *BioSystems*, vol. 87, no. 2, pp. 164–171, 2007.
- [14] R. Brette and W. Gerstner, "Adaptive exponential integrate-and-fire model as an effective description of neuronal activity," *Journal of neurophysiology*, vol. 94, no. 5, pp. 3637–3642, 2005.
- [15] R. Storn and K. Price, "Differential evolution—a simple and efficient heuristic for global optimization over continuous spaces," *Journal of global optimization*, vol. 11, no. 4, pp. 341–359, 1997.
- [16] S. Das and P. N. Suganthan, "Differential evolution: A survey of the state-of-the-art," *IEEE transactions on evolutionary computation*, vol. 15, no. 1, pp. 4–31, 2011.
- [17] M. E. H. Pedersen, "Good parameters for differential evolution," *Magnus Erik Hvass Pedersen*, 2010.
- [18] J. Brest, S. Greiner, B. Boskovic, M. Mernik, and V. Zumer, "Self-adapting control parameters in differential evolution: a comparative study on numerical benchmark problems," *IEEE transactions on evolutionary computation*, vol. 10, no. 6, pp. 646–657, 2006.
- [19] A. K. Qin, V. L. Huang, and P. N. Suganthan, "Differential evolution algorithm with strategy adaptation for global numerical optimization," *IEEE transactions on Evolutionary Computation*, vol. 13, no. 2, pp. 398–417, 2009.
- [20] E. Yavuz, J. Turner, and T. Nowotny, "Genn: a code generation framework for accelerated brain simulations," *Scientific reports*, vol. 6, 2016.
- [21] D. F. Goodman, M. Stimberg, P. Yger, and R. Brette, "Brian 2: neural simulations on a variety of computational hardware," *BMC Neuroscience*, vol. 15, no. 1, p. 1, 2014.
- [22] L. Salt, "Optimising a Neuromorphic Locust Looming Detector for UAV Obstacle Avoidance," Master's thesis, The University of Queensland, 2016.
- [23] A. W. Iorio and X. Li, "Solving rotated multi-objective optimization problems using differential evolution," in *Australasian Joint Conference on Artificial Intelligence*. Springer, 2004, pp. 861–872.
- [24] K. Eggensperger, M. Feurer, F. Hutter, J. Bergstra, J. Snoek, H. Hoos, and K. Leyton-Brown, "Towards an empirical foundation for assessing bayesian optimization of hyperparameters," in *NIPS workshop on Bayesian Optimization in Theory and Practice*, 2013, pp. 1–5.